

Coherence in resonance fluorescence

Xu-Jie Wang,¹ Guoqi Huang,^{1,2} Ming-Yang Li,³ Yuan-Zhuo Wang,³ Li Liu,¹ Bang Wu,^{1,*} Hanqing Liu,^{4,5} Haiqiao Ni,^{4,5} Zhichuan Niu,^{4,5} Weijie Ji,¹ Rongzhen Jiao,² Hua-Lei Yin,^{6,1,3,†} and Zhiliang Yuan^{1,‡}

¹Beijing Academy of Quantum Information Sciences, Beijing 100193, China

²School of Science, Beijing University of Posts and Telecommunications, Beijing 100876, China

³National Laboratory of Solid State Microstructures and School of Physics,

Collaborative Innovation Center of Advanced Microstructures, Nanjing University, Nanjing 210093, China

⁴State Key Laboratory of Superlattices and Microstructures,
Institute of Semiconductors, Chinese Academy of Sciences, Beijing 100083, China

⁵Center of Materials Science and Optoelectronics Engineering,
University of Chinese Academy of Sciences, Beijing 100049, China

⁶Department of Physics and Beijing Key Laboratory of Opto-electronic Functional Materials and Micro-nano Devices,
Key Laboratory of Quantum State Construction and Manipulation (Ministry of Education),
Renmin University of China, Beijing 100872, China

(Dated: June 3, 2024)

Resonance fluorescence (RF) of a two-level emitter displays persistently anti-bunching irrespective of the excitation intensity, but inherits the driving laser's linewidth under weak excitation. These properties are commonly explained *disjointedly* as the emitter's single photon saturation or passively scattering light, until a recent theory attributes anti-bunching to the laser-like spectrum's interference with the incoherently scattered light. However, the theory implies higher-order scattering processes, and led to an experiment purporting to validate an atom's simultaneous scattering of two photons. If true, it could complicate RF's prospects in quantum information applications. Here, we propose a unified model that treats all RF photons as spontaneous emission, one at a time, and can explain simultaneously both the RF's spectral and correlation properties. We theoretically derive the excitation power dependencies, with the strongest effects measurable at the single-photon incidence level, of the first-order coherence of the whole RF and super-bunching of the spectrally filtered, followed by experimental confirmation on a semiconductor quantum dot micro-pillar device. Furthermore, our model explains peculiar coincidence bunching observed in phase-dependent two-photon interference experiments. Our work provides novel understandings of coherent light-matter interaction and may stimulate new applications.

Although being a textbook phenomenon^{1–4}, resonance fluorescence (RF) remains an active research topic even in its simplest form^{5–11}. A two level emitter (TLE) under weak monochromatic excitation has been known to scatter out photons that are anti-bunched and yet exhibit the driving laser's linewidth^{12–16}. Anti-bunching was usually interpreted in the single-photon picture^{17,18}, i.e., a TLE absorbs and re-emits one photon at a time. However, this picture has not explained the origin of the RF's linewidth, which is far narrower than the natural broadening ($\frac{1}{2\pi T_1}$) imposed by the emitter's radiative lifetime (T_1). Conversely, it is easy to explain the laser-like spectrum if one treats the TLE only as a passive scattering site¹⁹, as often used for weak excitation, but explaining convincingly at the same time the RF's single-photon characteristic becomes challenging. Even more perplexing is the fact that the RF spectrum changes dramatically when the excitation intensity increases over a large range, but the single-photon characteristic persists^{10,11,20–22}, leading to greater difficulties with the two disjoint scattering pic-

tures.

Accompanying the spectrally sharp peak, RF spectrum of a TLE contains also a broadband component, which is vanishingly insignificant under weak excitation (Heitler regime) but grows towards dominance and eventually develops into Mollow triplets under strong excitation²³. Recently, a remarkable theoretical breakthrough by López Carreño et al.⁵ shows that it is the broadband component, however insignificant it may be, that holds the key to the presence or disappearance of anti-bunching through interference with the laser-like spectral component. Drastically departing from the single-photon picture, the broadband component was attributed to higher-order scattering processes involving “the actual *two-photon* absorption and re-emission”^{5,9}, which prompted experiments on the spectral filtering's effect on the photon number statistics^{6–8} and even led to suggestion of simultaneous scattering of two photons by an atom⁸. However, spectrally resolving the RF invokes interference among (many) photons emitted over a macroscopic duration no less than $1/\Delta\nu$ ($\Delta\nu$: spectral resolution), which would prevent discerning what truly happens at the minuscule duration of the TLE's radiative lifetime. From the perspective of wave-particle duality, the action of filtering reveals already the wave-aspect properties,

* wubang@baqis.ac.cn

† hlyin@ruc.edu.cn

‡ yuanzl@baqis.ac.cn

and thus undermines further discussions on simultaneity which requires treating photons as particles.

In this work, we propose and experimentally verify an entanglement model providing a unified picture which simultaneously explains the laser-like linewidth and the single-photon characteristics of the RF of a quantum emitter. Here, the emitter and its RF photons are entangled through spontaneous emission. The model involves no higher-order scattering processes, nor does it need to distinguish between “coherent” scattering and “incoherent” absorption/re-emission processes. From the entanglement, we theoretically derive the excitation power dependencies, with the strongest effects measurable at the single-photon incidence level, of the first-order coherence ($g^{(1)}$) of the RF as whole and the second-order correlation function ($g^{(2)}$) of its broadband component. In laboratory, we confirm the model by reproducing its predictions on the RF from a high-quality semiconductor quantum dot (QD) micro-pillar device. Furthermore, we perform phase-dependent two-photon interference experiment and observe peculiar coincidence bunching that is also explained by the model.

Figure 1a depicts the entanglement model. A monochromatic laser coherently drives a TLE, e.g., a QD in a micropillar cavity¹¹. Parameters ν , $h\nu$ and T_L are the laser’s frequency, photon energy and coherence time, respectively. The TLE’s excited state $|e\rangle$ has a lifetime of T_1 , and a dephasing time of T_2 ($T_2 \leq 2T_1$). According to the optical Bloch equations, the TLE population reaches a steady state after $\sim T_1$ time under steady continuous optical excitation¹. At any point of time, it is not possible to know whether spontaneous emission has taken place or the TLE remains at its excited state $|e\rangle$ prior to detection of a photon. However, once an RF photon is detected, we know for sure that spontaneous emission had taken place and the TLE returned to its ground state $|g\rangle$ at the corresponding point of time. An immediate detection of a second photon is prevented because the TLE

requires time to be repopulated. This leads naturally to photon anti-bunching.

To capture the above description, we write the light-matter system under *steady-state* condition as

$$|\psi\rangle_t = \sqrt{p_0}|0\rangle_t|g\rangle_t + \sqrt{p_1}e^{i2\pi\nu t}\frac{|0\rangle_t|e\rangle_t + |1\rangle_t|g\rangle_t}{\sqrt{2}}, \quad (1)$$

where p_0 and p_1 represent the TLE’s ground- and excited-state quasi-populations ($p_0 + p_1 = 1$), respectively. $|0\rangle_t|e\rangle_t$ means the TLE occupying its excited state has not spontaneously emitted at time t , while $|1\rangle_t|g\rangle_t$ indicates emission of a photon has just taken place with the TLE having returned to the ground state $|g\rangle_t$. We clarify that $|0\rangle_t$ and $|1\rangle_t$ here shall not be mistaken as cavity photons as in a Jaynes-Cummings-like model^{1,3,4}. States $|0\rangle_t|e\rangle_t$ and $|1\rangle_t|g\rangle_t$ are connected only via spontaneous emission, and $|1\rangle_t$ represents a spontaneously emitted photon into temporal mode t contributing to the RF. By definition, $|1\rangle_t$ is a broadband photon with bandwidth governed by the TLE’s dephasing time T_2 . Below, we show how the entanglement can transfer partially its coherence to the RF using two-path interference.

Figure 1b shows an asymmetric Mach-Zehnder interferometer (AMZI) with a delay τ ($T_1 \ll \tau \ll T_L$). The incoming RF signal from port a' is divided equally into two paths (a and b) by the first beam splitter and then recombine at the second one before detection at ports c and d by two single-photon detectors. When a photon is detected, it is not possible to distinguish whether it arose from a photon that was emitted to an early temporal mode ($t - \tau$) taking the long path or one emitted at a late mode (t) taking the short path. Interference between the two indistinguishable paths occurs. Since $\tau \gg T_1$, the two interfering temporal modes can be considered independent from each other, apart from their phase locked by the laser. Hence, we derive from equation (1) that the AMZI output at ports c and d to have the form

$$\begin{aligned} |\Psi_{\text{out}}\rangle = & |0_c 0_d\rangle_t \left(p_0 |gg\rangle + \frac{\sqrt{p_0 p_1}}{\sqrt{2}} |ge\rangle + \frac{\sqrt{p_0 p_1}}{\sqrt{2}} |eg\rangle + \frac{p_1}{2} |ee\rangle \right) \\ & + |1_c 0_d\rangle_t \frac{\sqrt{p_0 p_1}}{\sqrt{2}} \frac{1 - e^{i\varphi}}{\sqrt{2}} |gg\rangle + |1_c 0_d\rangle_t \frac{p_1}{2\sqrt{2}} (|ge\rangle - e^{i\varphi} |eg\rangle) - |2_c 0_d\rangle_t e^{i\varphi} \frac{p_1}{2\sqrt{2}} |gg\rangle \\ & + |0_c 1_d\rangle_t \frac{\sqrt{p_0 p_1}}{\sqrt{2}} \frac{1 + e^{i\varphi}}{\sqrt{2}} |gg\rangle + |0_c 1_d\rangle_t \frac{p_1}{2\sqrt{2}} (|ge\rangle + e^{i\varphi} |eg\rangle) + |0_c 2_d\rangle_t e^{i\varphi} \frac{p_1}{2\sqrt{2}} |gg\rangle. \end{aligned} \quad (2)$$

where φ denotes the AMZI phase delay and $|xy\rangle$ ($x, y = g, e$) represents the TLE’s respective states corresponding to time bins $t - \tau$ and t . The first line contains no photons while the second and third lines represent photon outputs at ports c and d , respectively. Each out-

put contains one phase-dependent term followed by two phase-independent ones. The phase-dependent term corresponds to the TLE’s transition $(|ge\rangle + |eg\rangle)/\sqrt{2} \rightarrow |gg\rangle$, which imparts the coherence to a superposition between two photon temporal modes: $(|0\rangle_{t-\tau} |1\rangle_t +$

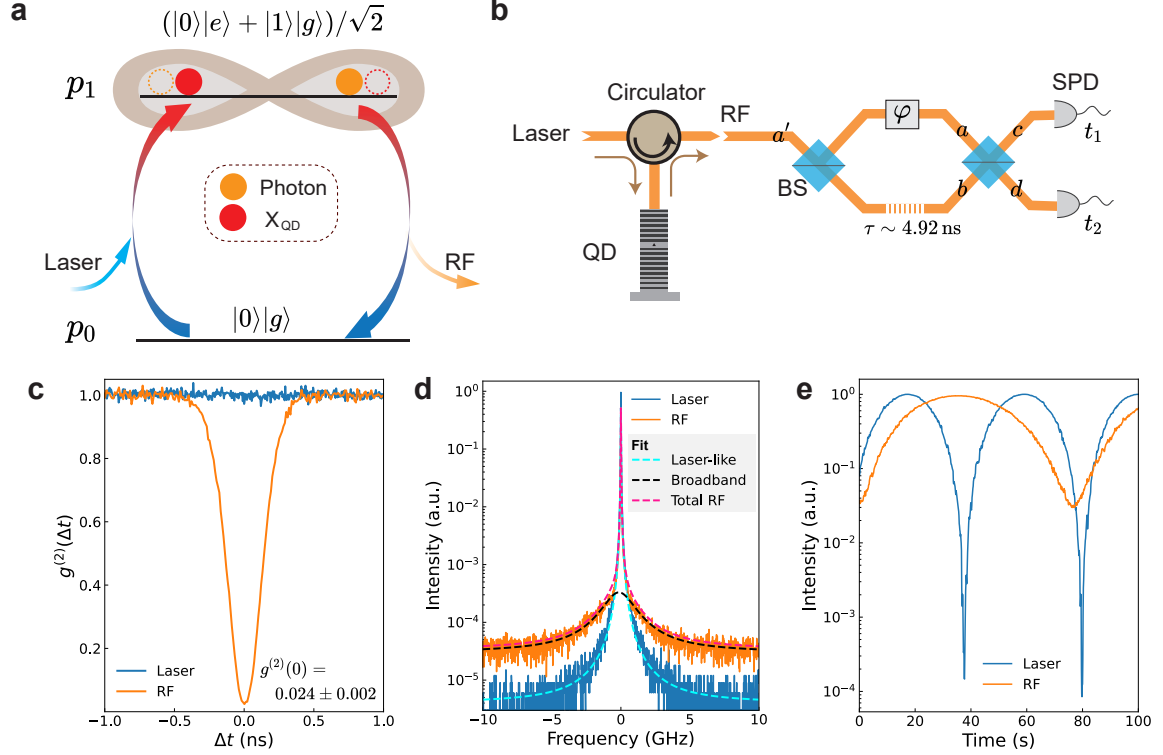


Fig. 1 | Resonance fluorescence (RF). **a**, Schematic for a two-level emitter (TLE) coherently driven by a continuous-wave laser into steady-state. Brackets $|g\rangle$ and $|e\rangle$ represent the ground and excited states of the TLE, while $|0\rangle$ and $|1\rangle$ mean 0 or 1 spontaneously emitted photon. Symbols p_0 represents the population of the system ground while p_1 is the single-quanta population that is in a form of either the TLE staying at its excited state ($|0\rangle|e\rangle$) or a fresh spontaneously emitted photon ($|1\rangle|g\rangle$). **b**, Schematic of the core experimental setup. **c**, Second-order correlation function $g^{(2)}(\Delta t)$ measurements. **d**, High resolution spectra. **e**, Interference fringes measured with the AMZI shown in **b**. The interferometer phase φ was left drifting freely. BS, beam splitter, SPD, single-photon detector.

$|1\rangle_{t-\tau}|0\rangle_t)/\sqrt{2}$. Varying the AMZI phase φ , this superposition will produce interference fringes with an amplitude of $\frac{p_0 p_1}{2}$, as opposed to the total output intensity of $\frac{p_1}{2}$. Thus, the coherence level of the RF, quantified using the first-order correlation function $g^{(1)}(\tau)$, has the form,

$$g^{(1)}(\tau) = p_0 e^{-i2\pi\nu\tau}. \quad (3)$$

Using Fourier transform, we infer that the RF consists of a spectrally sharp, laser-like (ll) part that inherits the linewidth of the driving laser and has a spectral weight of $I_{ll}/I_{tot} = |g^{(1)}(\tau)| = p_0 < 1$. For detailed theoretical derivation, see Sections I-III, Supplementary Information.

The reduction in coherence, by the amount of $1 - p_0$ or p_1 , is linked to the TLE's transitions from the $|ee\rangle$ state to $|ge\rangle$, $|eg\rangle$ or $|gg\rangle$. As shown in equation (2), the first two transitions give rise to an incoherent single photon each while the last one produces a two-photon state. Transition $|ee\rangle \rightarrow |ge\rangle$ ($|ee\rangle \rightarrow |eg\rangle$) emitted a photon

into early (late) temporal mode but none at late (early) mode, so no two-path interference takes place. On the other hand, transition $|ee\rangle \rightarrow |gg\rangle$ produces one photon into each mode, the interference of which causes coalescence and forms a photon-pair through Hong-Ou-Mandel (HOM) effect²⁴. All these photons are incoherent, so they naturally display a bandwidth governed by the TLE's transition and thus make up the broadband (bb) part, with a weight of $I_{bb}/I_{tot} = p_1$ in the RF spectrum.

In the absence of pure dephasing ($T_2 = 2T_1$), the relation of p_1 with excitation power can readily be estimated through steady-state condition. We define \bar{n} as the mean incident photon number over T_1 duration, and η_{ab} as the TLE's absorption/re-emission (scattering) efficiency under weak excitation limit. With absorption balancing out emission, we obtain $\frac{\bar{n}}{T_1} \times \eta_{ab} \times (1 - p_1) = \frac{p_1}{2} \times \frac{1}{T_1}$, where the factor $(1 - p_1)$ on the left takes saturation into account while $\frac{p_1}{2}$ on the right reflects on average only half

of the excited state is in the matter form. We then have

$$p_1 = 2\bar{n}\eta_{ab}/(1 + 2\bar{n}\eta_{ab}), \quad (4)$$

which provides a direct link with the excitation flux down to the single photon level, and has general applicability from deep Heitler ($\bar{n} \ll 1$) to high Mollow ($\bar{n} \gg 1$) regime. Since no assumption is made on the emitter type, we believe equation (4) holds, under the condition $T_2 = 2T_1$, for all quantum two-level emitters, including a trapped atom^{8,10} or ion¹², a molecule²⁰, and a semiconductor QD^{13–16,21,22}. The efficiency η_{ab} depends strongly how the excitation is coupled into the TLE. Previously, a transmission dip of 11.5 % was reported for a molecule under a freely propagating resonant excitation in a single-pass encounter without a cavity²⁰. Embedded an emitter into a cavity can enhance the light-matter interaction and could bring the scattering efficiency close to unity. For a high-quality QD-micropillar device^{11,25,26}, we expect $p_1 \approx \frac{2\bar{n}}{1+2\bar{n}}$ and $p_0 \approx \frac{1}{1+2\bar{n}}$, which presents a unique test-point to our model.

Equation (2) yields another experimentally verifiable prediction. By setting the AMZI's phase to $\varphi = \pi$, port d output contains two single-photon terms ($|1\rangle_t |ge\rangle$ and $|1\rangle_t |eg\rangle$) and a photon-pair term (with $|2\rangle_t |gg\rangle$). This output is equivalent to a pure two-photon state attenuated by a beam splitter. In the auto-correlation measurement, this state is expected to produce super-bunching that is dependent on the population p_1 : $g^{(2)}(0) = 1/p_1^2$. The derivation of this relation is summarised in Section IV of Supplementary Information.

Figure 1b shows the core experimental setup. We use a device containing a single InAs QD embedded in a micropillar cavity of 2.4 μm in diameter and a quality factor (Q) of 9350, featuring a low cavity resonance reflectivity of 0.015. It is kept in a closed-cycle cryostat and the QD's neutral exciton is temperature-tuned to resonate with the micropillar cavity at 13.6 K, emitting at 911.54 nm. We use a confocal microscope setup equipped with a tunable continuous-wave (CW) laser of 100 kHz linewidth as the excitation source and an optical circulator made of a polarising beam splitter and a quarter-wave plate for collecting the RF in a co-polarisation configuration¹¹. The QD is characterised to have a Purcell enhanced lifetime of $T_1 = 67.2$ ps ($F_p \simeq 10$), corresponding to a natural linewidth of $\Gamma_{\parallel}/2\pi = 2.37$ GHz, which is 15 times narrower than the cavity mode ($\kappa/2\pi = 35$ GHz). The RF is fed into a custom-built AMZI with a fixed delay of $\tau = 4.92$ ns for interference before detection by single photon detectors. With additional apparatuses, the whole setup allows characterisations of high-resolution spectroscopy, auto-correlation function $g^{(2)}(\Delta t)$, the first-order correlation function $g^{(1)}(\tau)$, and two-photon interference. For detailed description of the experimental setup, see Section VI of Information Section.

In the first experiment, we use a weak excitation flux of $\bar{n} = 0.0068$, corresponding to a Rabi frequency of $\Omega/2\pi = 210$ MHz ($\sim 0.09\Gamma_{\parallel}$). Here, the flux, defined as

$\bar{n} = P_{in}T_1/h\nu$, is strictly calibrated to represent the average number of photons incident upon the sample surface over T_1 duration. Figure 1c shows the auto-correlation function $g^{(2)}(\Delta t)$ for both the RF (orange line) and the laser (blue line). While the laser exhibits a flat $g^{(2)}$ because of its Poissonian statistics, the RF is strongly anti-bunched, with $g^{(2)}(0) = 0.024 \pm 0.002$, at the 0-delay over a time-scale of $\sim T_1$, confirming that the QD scatters one photon at a time.

Figure 1d shows the RF frequency spectrum (orange line) measured with a scanning Fabry-Pérot interferometer (FPI). It is dominated by a sharp line that overlaps the laser spectrum (blue line) with a linewidth that is limited by the FPI resolution (20 MHz). The RF contains additionally a broadband pedestal whose amplitude is over 3 orders of magnitude weaker. The overall spectrum can be excellently fit with two Lorentzians of 20 MHz and 2.3 GHz linewidths, shown as cyan and black dashed lines, respectively. The bandwidth of the latter closely matches the TLE's natural linewidth of $\Gamma_{\parallel}/2\pi$. Following the discussion surrounding equation (3), we attribute the sharp feature to the interference outcome of the RF signal passing through the FPI. The spectral weight of this laser-like peak can be measured using our AMZI (Fig. 1b), which has a suitable delay that meets the condition $T_1 \ll \tau \ll T_L$. An example result is shown in Fig. 1e, which gives a fringe visibility, or the laser-like fraction, of 0.94 for the RF. As comparison, the laser signal exhibits 0.9998 interference visibility.

Figure 2a shows high-resolution RF spectra under different excitation fluxes. As the flux increases, the broadband component increases its share of the total RF, and becomes considerably broadened when \bar{n} exceeds 0.25. It starts to develop into Mollow triplets at the few photon level as reported previously¹¹. Nevertheless, the RF remains its single-photon characteristics for a flux up to $\bar{n} = 6.8$ when measured before the AMZI and *without any spectral filtering*, as demonstrated by the auto-correlation data (open squares) in Fig. 2b. At $\bar{n} = 6.8$, we measure $g^{(2)}(0) = 0.37$, which is still below the limit (0.5) for a classical emitter.

The growing broadband component deteriorates the RF's coherence. To quantify, we measure the interference visibility ($|g^{(1)}|$) by passing the RF through the AMZI, with results shown as solid circles in Fig. 2b. This quantification method is equivalent to, and more precise than, calculating the area ratio of the laser-like peak to the total RF signal. The results from the latter method are shown as stars. At low fluxes ($\bar{n} < 0.01$), $|g^{(1)}|$ is plateaued at 0.946, rather than 1.0 as expected from equation (3). We attribute this discrepancy to photon distinguishability²⁷, which could arise from phonon-scattering^{28–30} and QD environmental charge fluctuation³¹ as well as a small amount of laser mixed into the RF. As the flux increases until $\bar{n} = 3$, we observe a general trend of a decreasing visibility. For $\bar{n} > 3.0$, the visibility reverses its downward trend and climbs up. In this regime, the RF signal starts to saturate¹¹ while the laser

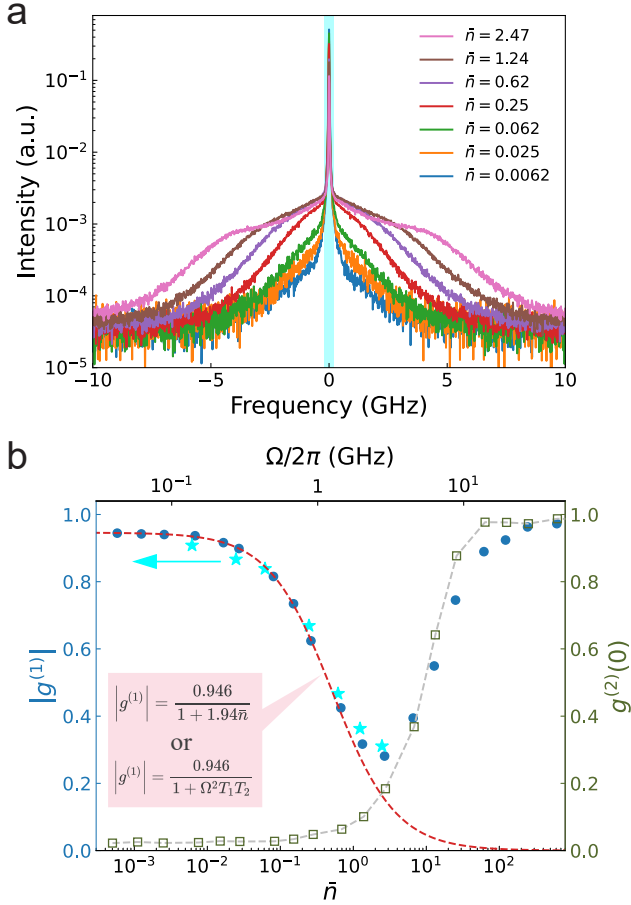


Fig. 2 | Coherence versus excitation flux at the single-photon level. **a**, High-resolution RF spectra; The cyan bar illustrates the laser-like spectral part. **b**, The interference visibility $|g^{(1)}|$ (solid circles) measured with the AMZI (see Fig. 1b), the laser-like spectral weight I_l/I_{tot} (solid stars) extracted from data in panel **a**, and the auto-correlation measured without any spectral filtering. The red dashed line is a fitting using either $|g^{(1)}| \propto \frac{1}{1+x\bar{n}}$ with $x = 1.94$ or $|g^{(1)}| \propto \frac{1}{1+\Omega^2 T_1 T_2}$ with $T_2 = 1.62T_1$.

background continues to rise, as evidenced by the accompanying rise in $g^{(2)}(0)$. At very strong fluxes ($\bar{n} > 100$), the laser background dominates and thus the measured photon number statistics approaches Poissonian distribution, i.e., $g^{(2)}(0) \approx 1$.

We attribute the interference visibility drop in Fig. 2b to the increasing population (p_1) of the QD's exited state. Based on equations (3, 4), we obtain a near perfect fit, $|g^{(1)}| = 0.946/(1+x\bar{n})$ and $x = 1.94$, to the experimental data in the region where the RF signal remains dominant. It is also viable to fit the $g^{(1)}$ data using the traditional model^{2,13,26}: $|g^{(1)}| \propto \frac{1}{1+\Omega^2 T_1 T_2}$, the result of which is represented also by the dashed line. In the fitting, we use $T_2 = 1.62T_1$ and extrapolate the Rabi frequencies from the splittings in Mollow spectral triplets measured un-

der strong excitation. While both models work, ours is substantially simpler in the sense that it links the RF's coherence directly to the incident flux down the single photon excitation level. This experiment gives strong support to our simple model and at the same time suggests an efficient coupling of light into our QD-micropillar device.

In the next experiment (Fig. 3a), we use the AMZI to filter out the laser-like component by setting its phase to $\varphi = \pi$ and then study the photon number statistics of the filtered RF output. As compared with a narrow-band filter⁶⁻⁸, this technique uses two-path, instead of multi-path, interference and thus the subsequent photon number statistics is easier to analyse. For the theoretical analysis, see Section IV of Supplementary Information. Two AMZI-filtered spectra are shown in Fig. 3b. Each spectrum consists of a broadband signal with fringes of 203 MHz spacing corresponding to the AMZI's delay ($\tau = 4.92$ ns), while the laser-like component is rejected entirely. Subjecting the filtered RF to the auto-correlation measurement, we acquire a set of data shown in Fig. 3c. We observe super-bunching at 0-delay with $g^{(2)}(0) = 168.9$ at the lowest flux of $\bar{n} = 0.0062$, and attribute it to two-photon interference between an early single photon passing through the long arm and a late one passing through the short arm of the AMZI. At $\Delta t = \pm\tau$, interference between three temporal modes happens. Theoretically, $g^{(2)}(\pm\tau) \approx \frac{1}{4}g^{(2)}(0)$ under such incident flux. To compare, we have measured an average value of 47.6 for $g^{(2)}(\pm\tau)$, amounting to 0.282 of the corresponding $g^{(2)}(0)$ value.

The level of super-bunching decreases with the excitation photon flux, as shown in Fig. 3c. This is in qualitative agreement with the theoretical prediction of $g^{(2)}(0) = 1/p_1^2$. At $\bar{n} = 0.62$, we deduce $p_1 = 0.546$ using $p_1 = 1.94\bar{n}/(1 + 1.94\bar{n})$ and thus expect a photon bunching value of 3.35. Experimentally, we obtain $g^{(2)}(0) = 2.6$, which is in fair agreement with the expected value. The discrepancy could arise from the increased laser background as well as finite photon indistinguishability²⁷.

Finally, we perform phase-dependent two-photon interference experiment with the setup shown in Fig. 1b, and summarize the results in Fig. 4a with observations: (1) The coincidence baseline is phase-dependent, while the gap between traces shrinks as the excitation power increases; (2) Strong anti-bunching at $\Delta t = 0$ for all excitation fluxes and phase values; (3) Features at $\Delta t = \pm 4.92$ ns, caused by the AMZI's delay τ , can exhibit as peaks or dips depending on both the excitation power and the phase delay. We note that observation (3) is strikingly different from incoherently excited quantum emitters^{26,32}, where the side features always display as dips with depth limited to 0.75.

To understand the two-photon interference results, we approximate the RF output as a superposition of photon-number states: $|\psi_{ph}\rangle_t = \sqrt{p_0}|0\rangle_t + \sqrt{p_1}|1\rangle_t + \sqrt{p_2}|2\rangle_t$ with a small two-photon probability $p_2 \ll p_1^2/2$ and derive the

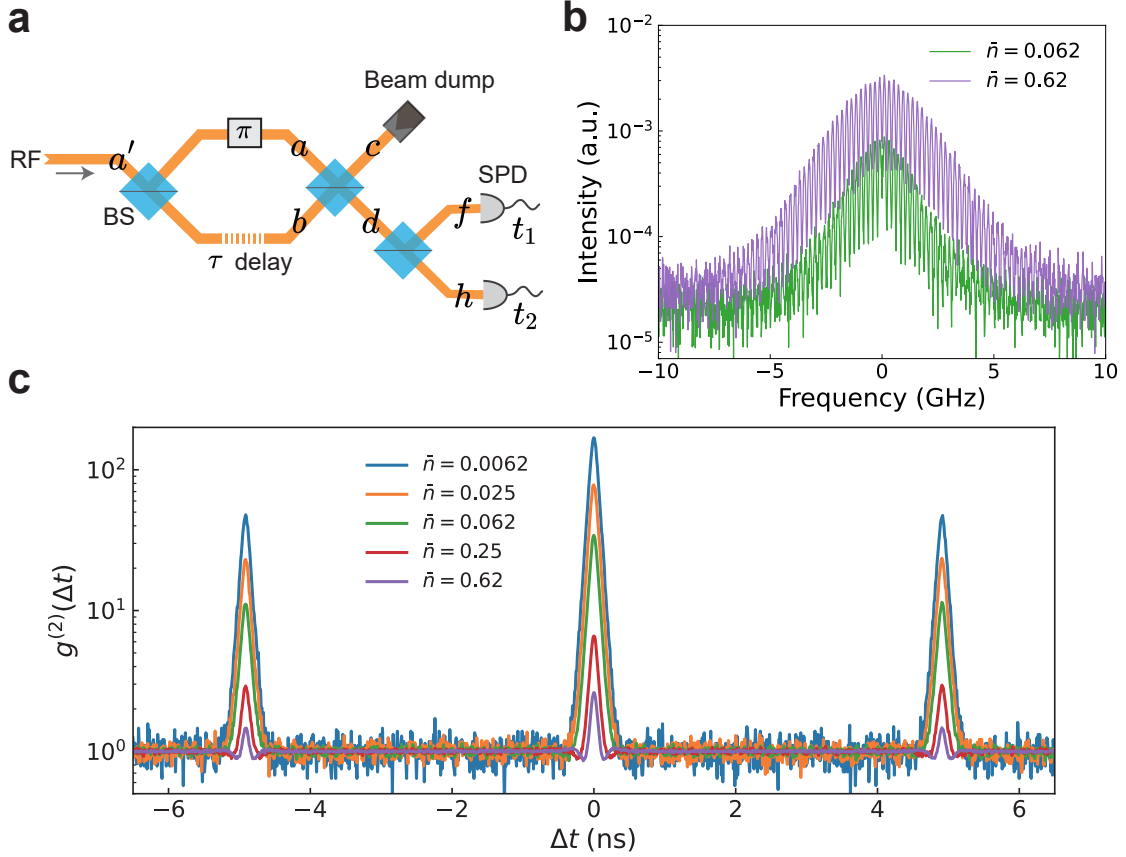


Fig. 3 | Correlation of the AMZI-filtered RF. **a**, Experimental setup; The AMZI is set to have a π phase so that the laser-like RF coherent is dumped at port c ; The filtered RF at port d contains only broadband RF, and is fed into a HBT setup. **b**, Filtered RF spectra; **c**, Second-order correlation functions measured for various excitation fluxes.

coincidence probabilities as detailed in Section V of Supplementary Information. We reproduce the main results below.

$$\mathcal{C}(0) = \frac{p_2}{4} (1 - p_0 M \cos 2\varphi) + \frac{p_1^2 + 4p_1 p_2 + 4p_2^2}{8} (1 - M'), \quad (5A)$$

$$\mathcal{C}(\pm\tau) = \frac{p_1^2}{16} (3 - 2p_0 M \cos 2\varphi), \quad (5B)$$

$$\mathcal{C}_0 = \frac{p_1^2}{4} (1 - p_0^2 M \cos^2 \varphi), \quad (5C)$$

where M represents indistinguishability of the RF photons while M' is the post-selective two-photon interference visibility with detector jitter taken into account³³. $\mathcal{C}(\Delta t)$ represents the coincidence probability at time interval Δt while \mathcal{C}_0 is the baseline coincidence. Equations (5A-5C) show all coincidence probabilities are phase-dependent. \mathcal{C}_0 and $\mathcal{C}(\pm\tau)$'s dependence arises from the first-order interference, while $\mathcal{C}(0)$ contains contributions

from $|2\rangle_t$ states as well as incomplete HOM interference between two RF photons emitted separately by the AMZI delay τ . Figures 4b, 4c plot the phase dependence of the theoretical (solid lines) and experimental (symbols) coincidence rates for $\Delta t = \pm\tau$ and $\Delta t = 0$, normalised to the baseline coincidence. We use maximum likelihood estimation method to determine a realistic set of parameters for each excitation flux that provide the best fit to the data. The theoretical simulations are in excellent agreement with the experimental data for three incident fluxes and have also successfully reproduced the crossover between $\mathcal{C}(\pm\tau)$ and \mathcal{C}_0 for $\bar{n} = 0.25$.

Over past 50 years, it has been prevalent to discuss resonance fluorescence in the context of “coherently” and “incoherently” scattered light^{5–9,13,14,23}. In literature, interchangeable terminologies, such as resonant Rayleigh scattering (RRS) vs. resonant photoluminescence (RPL)²⁶ and elastic vs. inelastic scattering³⁴, are also in use. The term “incoherent scattering” is rather misleading. As we have elucidated, both the laser-like and broadband parts arise from the very same coherent process, i.e., resonant absorption and spontaneous emis-

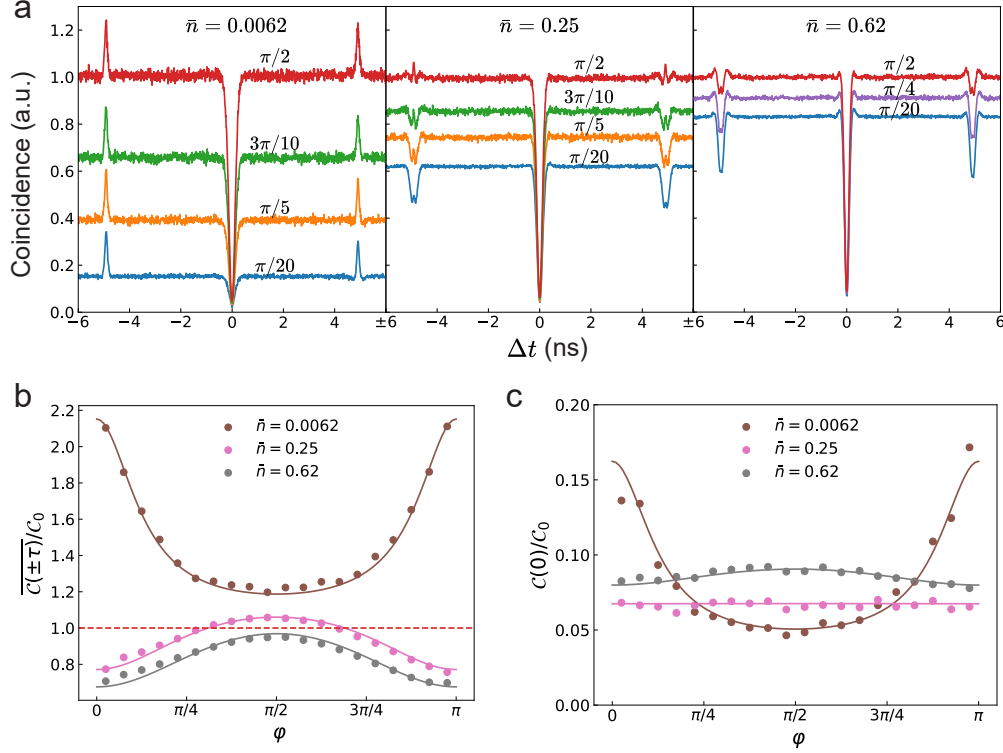


Fig. 4 | Phase-dependent two-photon interference. **a**, Cross-correlation traces measured with the setup shown in Fig. 1b for three different excitation intensities: $\bar{n} = 0.0062$ (left), 0.25 (middle) and 0.62 (right panel). **b**, Measured (solid symbols) and theoretical (solid lines) coincidence probabilities at $\Delta t = \pm\tau$ delays, normalised to the coincidence baseline (dashed line). We use $\overline{C(\pm\tau)} = \frac{1}{2} (C(+\tau) + C(-\tau))$. **c**, Normalised experimental (solid symbols) and theoretical (solid lines) coincidence probabilities at $\Delta t = 0$. Experimental data in panels **b** and **c** are extracted from data in panel **a**. The theoretical results are fitted using maximum likelihood estimation based on equations (5A)~(5C). Fitted parameters $\{p_0, p_1, p_2; M'\}$ corresponding to different excitation fluxes $\bar{n} = 0.0062, 0.25, 0.62$ are $\{0.98, 0.023, 8.0 \times 10^{-6}; 0.96\}$, $\{0.69, 0.30, 2.2 \times 10^{-3}; 0.94\}$ and $\{0.49, 0.50, 8.0 \times 10^{-3}; 0.92\}$, respectively. A fixed value of $M = 0.89$, extracted from the plateaued $|g^{(1)}| = 0.946$ shown in Fig. 2b through $M = |g^{(1)}|^2$, is used for photon indistinguishability.

sion. The two parts are integral. Their integrity is key to the joint observation of “sub-natural” linewidth and anti-bunching. Conversely, compromise in the integrity will change the photonic state and may lead to different observations, e.g., loss of anti-bunching after spectral filtering^{6–8} or super-bunching after the AMZI filtering (Fig. 3). We stress that photon bunching does not necessarily require simultaneous scattering of two photons⁸ for an explanation.

To conclude, we have presented a novel picture to explain the coherence of resonance fluorescence under

continuous-wave excitation. We link the RF’s coherence to the incident flux down to the single-photon level and show how to manipulate photon number statistics through simple two-path interference. We clarify that coherent scattering can be treated as a process of absorption and re-emission and does not need to involve higher-order scattering processes to explain experiments. Our work adds clarity to the knowledge pool of RF-based quantum light sources and we believe it will help foster new applications. One opportunity is to exploit the RF’s coherence for quantum secure communication^{35,36}.

1. Steck, D. A. Quantum and atom optics. [http://steck.us/teaching\(revision0.14,23August2023\)](http://steck.us/teaching(revision0.14,23August2023)).
2. Loudon, R. *The quantum theory of light* (OUP Oxford, 2000).
3. Fox, M. *Quantum Optics: An Introduction* (Oxford University Press, Oxford, 2006).

4. Grynberg, G., Aspect, A., Fabre, C. & Cohen-Tannoudji, C. *Introduction to Quantum Optics: From the Semi-classical Approach to Quantized Light* (Cambridge University Press, 2010).
5. López Carreño, J. C., Zubizarreta Casalengua, E., Laussy, F. P. & del Valle, E. Joint subnatural-linewidth

- and single-photon emission from resonance fluorescence. *Quant. Sci. Technol.* **3**, 045001 (2018).
6. Phillips, C. L. *et al.* Photon statistics of filtered resonance fluorescence. *Phys. Rev. Lett.* **125**, 043603 (2020).
 7. Hanschke, L. *et al.* Origin of antibunching in resonance fluorescence. *Phys. Rev. Lett.* **125**, 170402 (2020).
 8. Masters, L. *et al.* On the simultaneous scattering of two photons by a single two-level atom. *Nat. Photon.* **17**, 972–976 (2023).
 9. Casalengua, E. Z., Laussy, F. P. & del Valle, E. Two photons everywhere. *arXiv preprint arXiv:2402.14010* (2024).
 10. Ng, B. L., Chow, C. H. & Kurtsiefer, C. Observation of the Mollow triplet from an optically confined single atom. *Phys. Rev. A* **106**, 063719 (2022).
 11. Wu, B. *et al.* Mollow triplets under few-photon excitation. *Optica* **10**, 1118 – 1123 (2023).
 12. Höffges, J., Baldauf, H., Eichler, T., Helmfrid, S. & Walther, H. Heterodyne measurement of the fluorescent radiation of a single trapped ion. *Opt. Commun.* **133**, 170–174 (1997).
 13. Nguyen, H.-S. *et al.* Ultra-coherent single photon source. *Appl. Phys. Lett.* **99**, 261904 (2011).
 14. Konthasinghe, K. *et al.* Coherent versus incoherent light scattering from a quantum dot. *Phys. Rev. B* **85**, 235315 (2012).
 15. Matthiesen, C., Vamivakas, A. N. & Atatüre, M. Subnatural linewidth single photons from a quantum dot. *Phys. Rev. Lett.* **108**, 093602 (2012).
 16. Matthiesen, C. *et al.* Phase-locked indistinguishable photons with synthesized waveforms from a solid-state source. *Nat. Commun.* **4**, 1600 (2013).
 17. Carmichael, H. J. & Walls, D. F. Proposal for the measurement of the resonant stark effect by photon correlation techniques. *J. Phys. B At. Mol. Opt. Phys.* **9**, L43 (1976).
 18. Kimble, H. J., Dagenais, M. & Mandel, L. Photon antibunching in resonance fluorescence. *Phys. Rev. Lett.* **39**, 691–695 (1977).
 19. Lodahl, P., Mahmoodian, S. & Stobbe, S. Interfacing single photons and single quantum dots with photonic nanostructures. *Rev. Mod. Phys.* **87**, 347–400 (2015).
 20. Wriggle, G., Gerhardt, I., Hwang, J., Zumofen, G. & Sandoghdar, V. Efficient coupling of photons to a single molecule and the observation of its resonance fluorescence. *Nat. Phys.* **4**, 60–66 (2008).
 21. Flagg, E. B. *et al.* Resonantly driven coherent oscillations in a solid-state quantum emitter. *Nat. Phys.* **5**, 203–207 (2009).
 22. Ates, S. *et al.* Post-Selected Indistinguishable Photons from the Resonance Fluorescence of a Single Quantum Dot in a Microcavity. *Phys. Rev. Lett.* **103**, 167402 (2009).
 23. Mollow, B. R. Power spectrum of light scattered by two-level systems. *Phys. Rev.* **188**, 1969–1975 (1969).
 24. Hong, C. K., Ou, Z. Y. & Mandel, L. Measurement of subpicosecond time intervals between two photons by interference. *Phys. Rev. Lett.* **59**, 2044–2046 (1987).
 25. De Santis, L. *et al.* A solid-state single-photon filter. *Nat. Nanotech.* **12**, 663–667 (2017).
 26. Proux, R. *et al.* Measuring the photon coalescence time window in the continuous-wave regime for resonantly driven semiconductor quantum dots. *Phys. Rev. Lett.* **114**, 067401 (2015).
 27. Lored, J. *et al.* Generation of non-classical light in a photon-number superposition. *Nat. Photon.* **13**, 803–808 (2019).
 28. Iles-Smith, J., McCutcheon, D. P. S., Nazir, A. & Mørk, J. Phonon scattering inhibits simultaneous near-unity efficiency and indistinguishability in semiconductor single-photon sources. *Nat. Photon.* **11**, 521–526 (2017).
 29. Koong, Z. X. *et al.* Fundamental limits to coherent photon generation with solid-state atomlike transitions. *Phys. Rev. Lett.* **123**, 167402 (2019).
 30. Brash, A. J. *et al.* Light scattering from solid-state quantum emitters: Beyond the atomic picture. *Phys. Rev. Lett.* **123**, 167403 (2019).
 31. Zhai, L. *et al.* Low-noise GaAs quantum dots for quantum photonics. *Nat. Commun.* **11**, 4745 (2020).
 32. Patel, R. B. *et al.* Postselective two-photon interference from a continuous nonclassical stream of photons emitted by a quantum dot. *Phys. Rev. Lett.* **100**, 207405 (2008).
 33. Legero, T., Wilk, T., Hennrich, M., Rempe, G. & Kuhn, A. Quantum beat of two single photons. *Phys. Rev. Lett.* **93**, 070503 (2004).
 34. Metcalfe, M., Solomon, G. S. & Lawall, J. Heterodyne measurement of resonant elastic scattering from epitaxial quantum dots. *Appl. Phys. Lett.* **102**, 231114 (2013).
 35. Zhou, L. *et al.* Experimental quantum communication overcomes the rate-loss limit without optical phase tracking. *Phys. Rev. Lett.* **130**, 250801 (2023).
 36. Karli, Y. *et al.* Controlling the photon number coherence of solid-state quantum light sources for quantum cryptography. *npj Quant. Inf.* **10**, 17 (2024).

Data availability

All the data that support the plots within this manuscript and other findings of this study are available from the corresponding authors upon reasonable request.

Acknowledgements

Z.Y. acknowledges helpful discussions with Z. Q. Yin, Y. K. Wu, Y. Ji and X. B. Wang. This work was supported by the National Natural Science Foundation of China under grants 12204049 (X.-J.W.), 12274223 (H.-L.Y.) and 62250710162 (Z.Y.), National Key R & D Program of China under grant 2018YFA0306101 (Z.N.), and Beijing Natural Science Foundation under grant IS23011 (Z.Y.).

Author contributions

Z.Y., X.-J.W. and B.W. designed the research. X.-J.W., G.H. and B.W. carried out the experiments. H.-L.Y., M.-Y.L., Y.-Z.W., and X.-J.W. developed the theoretical derivation and performed the simulations. L.L. fabricated the devices with assistance from W.J. H.L., H.N. and Z.N. grew the semiconductor wafer. X.-J.W. and Z.Y. prepared the manuscript with input from all authors. Z.Y. conceived the model and supervised the project.

Competing interests

The authors declare no competing interests.

Supplementary Information for “Coherence in Resonance Fluorescence”

Xu-Jie Wang,¹ Guoqi Huang,^{1,2} Ming-Yang Li,³ Yuan-Zhuo Wang,³ Li Liu,¹ Bang Wu,^{1,*} Hanqing Liu,^{4,5} Haiqiao Ni,^{4,5} Zhichuan Niu,^{4,5} Weijie Ji,¹ Rongzhen Jiao,² Hua-Lei Yin,^{6,1,3,†} and Zhiliang Yuan^{1,‡}

¹*Beijing Academy of Quantum Information Sciences, Beijing 100193, China*

²*School of Science, Beijing University of Posts and Telecommunications, Beijing 100876, China*

³*National Laboratory of Solid State Microstructures and School of Physics,*

Collaborative Innovation Center of Advanced Microstructures, Nanjing University, Nanjing 210093, China

⁴*State Key Laboratory of Superlattices and Microstructures, Institute of Semiconductors, Chinese Academy of Sciences, Beijing 100083, China*

⁵*Center of Materials Science and Optoelectronics Engineering, University of Chinese Academy of Sciences, Beijing 100049, China*

⁶*Department of Physics and Beijing Key Laboratory of Opto-electronic Functional Materials and Micro-nano Devices, Key Laboratory of Quantum State Construction and Manipulation (Ministry of Education), Renmin University of China, Beijing 100872, China*

(Dated: June 3, 2024)

I. CHANNEL LOSS

In any resonance fluorescence (RF) setup, there is inevitably channel loss from the source to the final detection. Here we prove that the channel loss does not affect the analysis of the first or second-order correlation functions, irrespective whether the light field is described by a pure or a mixed state.

Consider a quantum channel with transmission efficiency η , the corresponding light field operator transformation relation is

$$x_t \rightarrow \sqrt{\eta}y_t + \sqrt{1-\eta}z_t, \quad (\text{S.1})$$

where x_t is annihilation operator of the input light field, y_t and z_t are the annihilation operator of transmission and reflection part in quantum channel, respectively. Tracing over mode z_t leads to:

$$\begin{aligned} \langle x_{t'}^\dagger x_t \rangle &\rightarrow \eta \langle y_{t'}^\dagger y_t \rangle, \\ \langle x_t^\dagger x_t \rangle &\rightarrow \eta \langle y_t^\dagger y_t \rangle, \\ \langle x_t^\dagger x_{t'}^\dagger x_{t'} x_t \rangle &\rightarrow \eta^2 \langle y_t^\dagger y_{t'}^\dagger y_{t'} y_t \rangle. \end{aligned} \quad (\text{S.2})$$

Then, we can calculate the first-order correlation function

$$g^{(1)}(\tau) = \frac{\langle x_{t+\tau}^\dagger x_t \rangle}{\langle x_t^\dagger x_t \rangle} = \frac{\langle y_{t+\tau}^\dagger y_t \rangle}{\langle y_t^\dagger y_t \rangle}, \quad (\text{S.3})$$

and the second-order correlation function

$$g^{(2)}(\tau) = \frac{\langle x_t^\dagger x_{t+\tau}^\dagger x_{t+\tau} x_t \rangle}{\langle x_t^\dagger x_t \rangle^2} = \frac{\langle y_t^\dagger y_{t+\tau}^\dagger y_{t+\tau} y_t \rangle}{\langle y_t^\dagger y_t \rangle^2}. \quad (\text{S.4})$$

Equations (S.3, S.4) mean that channel loss does not affect the analysis of the first- or second-order correlation functions. Therefore, we will ignore all channel losses in our subsequent derivation of the RF's coherence.

II. THE FIRST-ORDER CORRELATION FUNCTION $g^{(1)}(\tau)$ AND OPTICAL FREQUENCY SPECTRUM OF RESONANCE FLUORESCENCE

The first-order correlation function $g^{(1)}(\tau)$ characterises the coherence of an optical field¹. It measures the normalised interference outcome of an optical field with its delayed copy by time τ ,

$$g^{(1)}(\tau) = \frac{\langle \hat{E}_{t+\tau}^{(-)} \hat{E}_t^{(+)} \rangle}{\langle \hat{E}_t^{(-)} \hat{E}_t^{(+)} \rangle}, \quad (\text{S.5})$$

where $\hat{E}_t^{(+)} = E_0 a_t'$ and $\hat{E}_t^{(-)} = E_0 a_t'^{\dagger}$ with a_t' and $a_t'^{\dagger}$ being photon annihilation and creation operators and E_0 the electric field per photon. A light source is said to be incoherent if $|g^{(1)}(\tau)| = 0$ and coherent if $|g^{(1)}(\tau)| = 1$ for $\tau \neq 0$. For example, a monochromatic light is perfectly coherent as $|g^{(1)}(\tau)| \equiv 1$. With knowledge of its $g^{(1)}(\tau)$, the frequency spectrum of a light source can be calculated using Wiener-Khinchin theorem,

$$I(\nu) = \int_0^\infty g^{(1)}(\tau) e^{i2\pi\nu\tau} d\tau, \quad (\text{S.6})$$

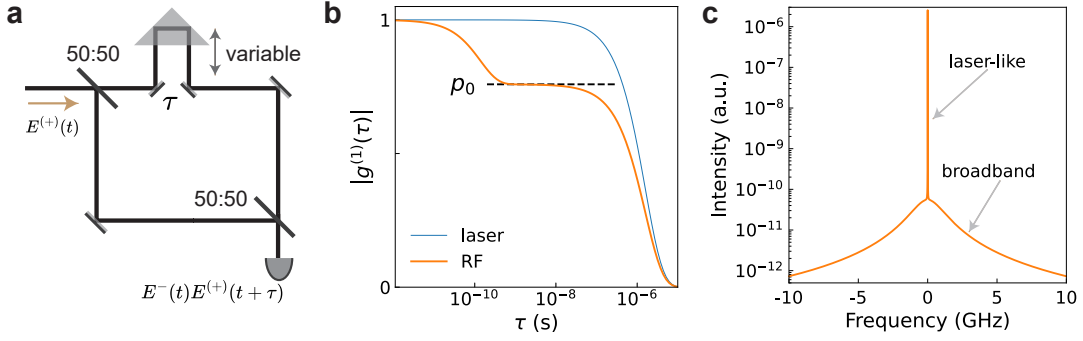
where ν denotes optical frequency. A coherent source has a δ -function like spectrum. Experimentally, $g^{(1)}(\tau)$ can be measured through an asymmetric Mach-Zehnder interferometer (AMZI) with a variable delay τ , as schematically shown in Supplementary Fig. 1a. Its absolute value represents the interference visibility: $V \equiv |g^{(1)}(\tau)|$.

We now derive the first-order correlation function for the RF of a quantum two-level emitter (TLE) driven by a continuous-wave laser with a coherence time of T_L . Here, we start with an ideal scenario, i.e., the emitter is free

* wubang@baqis.ac.cn

† hlyin@ruc.edu.cn

‡ yuanzl@baqis.ac.cn



Supplementary Fig. 1. The first-order coherence function and optical frequency spectrum. **a**, An experimental schematic diagram that can be used to measure first-order correlation function $g^{(1)}(\tau)$. **b**, Theoretical $g^{(1)}(\tau)$ of RF under a finite excitation power. The curve reveals that the double-exponential decay of $|g^{(1)}(\tau)| = p_1 \exp(-\tau/T_2) + p_0 \exp(-\tau/T_L)$. As a comparison, we also provide the theoretical $|g^{(1)}(\tau)| = \exp(-\tau/T_L)$ of the laser. **c**, RF spectrum obtained by performing Fourier transform on the first-order correlation function $|g^{(1)}(\tau)|$ shown in panel **b**. The laser-like component of the spectrum corresponds to the slowly decaying portion in $|g^{(1)}(\tau)|$, while the broadband corresponds to the rapidly decaying portion of $|g^{(1)}(\tau)|$. In the calculation, we use $T_2 = 137.4$ ps and $T_L = 1.59$ μ s, corresponding to our experimental parameters of QD's lifetime of 67.2 ps and the laser's linewidth of 100 kHz.

from any extrinsic dephasing process ($T_2 = 2T_1$), and the RF signal is free from any laser background. As proposed in Main Text, we write the entangled state between the RF and the TLE under steady-state condition as

$$|\psi\rangle_t = \sqrt{p_0} |0\rangle_t |g\rangle_t + \sqrt{p_1} e^{i2\pi\nu t} \frac{|0\rangle_t |e\rangle_t + |1\rangle_t |g\rangle_t}{\sqrt{2}}, \quad (\text{S.7})$$

where $|0\rangle_t$ denotes vacuum state while $|1\rangle_t$ represents a single photon emitted into temporal mode t . $p_0 + p_1 = 1$ and with optical excitation we have $p_0 < 1$.

Plugging the above light-matter state into equations (S.3) and (S.4) for $T_1 \ll \tau \ll T_L$, we obtain the first-order correlation function,

$$g^{(1)}(\tau) = \frac{\langle \psi |_{t+\tau} \langle \psi |_t a_{t+\tau}^\dagger a'_t | \psi \rangle_t | \psi \rangle_{t+\tau}}{\langle \psi |_t a_t^\dagger a'_t | \psi \rangle_t} = p_0 e^{-i2\pi\nu\tau}, \quad (\text{S.8})$$

and the second-order correlation function

$$g^{(2)}(0) = \frac{\langle \psi |_t a_t^\dagger a_t'^\dagger a'_t a'_t | \psi \rangle_t}{\langle \psi |_t a_t^\dagger a'_t | \psi \rangle_t^2} = 0, \quad (\text{S.9})$$

where a_t^\dagger and $a_{t+\tau}^\dagger$ act in quantum states $|\psi\rangle_t$ and $|\psi\rangle_{t+\tau}$, respectively. The RF has a finite coherence ($p_0 < 1$) and simultaneously photon anti-bunching, which is in agreement with experiments.

For short delays, i.e., $\tau \in [0, T_2]$, the first-order correlation function measures the interference of each RF photon with itself. Therefore, $g^{(1)}$ is governed by the TLE's dephasing time T_2 under weak excitation, and will become mediated by the Rabi oscillation under strong excitation. Then, we have $|g^{(1)}(0)| = 1$ at $\tau = 0$, followed by a fast decay to the plateaued value of p_0 . When τ becomes comparable to or exceeds the laser coherence time T_L , $|g^{(1)}(\tau)|$ will start its second exponential decay. The overall dependence on τ is illustrated in Fig. 1b.

Through Fourier transform, we can calculate the RF frequency spectrum as shown in Supplementary Fig. 1c. Closely resembling the experimental data (Fig. 1d, Main Text), the spectrum contains a sharp peak that inherits the laser linewidth and a broadband pedestal of the TLE's bandwidth. The laser-like (ll) part has a spectral weight of $I_{ll}/I_{tot} = |g^{(1)}(\tau)| = p_0 < 1$.

III. ORIGIN OF THE RF'S COHERENCE AND ITS PARTIAL LOSS

To reveal how the RF obtains or loses its coherence, we derive the interference outcome when passing it through an AMZI ($T_1 \ll \tau \ll T_L$). As two-path interference occurs between a late temporal mode $|\psi\rangle_t$ passing through the short arm and an early mode $|\psi\rangle_{t-\tau}$ through the long arm, we derive from equation (S.7) the joint input state between two temporal modes as a tensor product

$$|\psi\rangle_{t-\tau} |\psi\rangle_t = |00\rangle \left[p_0 |gg\rangle + \frac{\sqrt{p_0 p_1}}{\sqrt{2}} (|ge\rangle + |eg\rangle) + \frac{p_1}{2} |ee\rangle \right] + \frac{\sqrt{p_0 p_1}}{\sqrt{2}} |gg\rangle (|10\rangle + |01\rangle) + \frac{p_1}{2} (|10\rangle |ge\rangle + |01\rangle |eg\rangle) + \frac{p_1}{2} |11\rangle |gg\rangle, \quad (\text{S.10})$$

where all time evolution phases are dropped for clarity. State $|01\rangle$ represents 0-photon at temporal mode $t - \tau$ and 1-photon at mode t , state $|ge\rangle$ denotes the TLE occupying the ground state at time $t - \tau$ and the excited state at time t . All other bracket states are defined in the same way.

The first term in equation (S.10) contains no photons. The second term contains $|10\rangle + |01\rangle$, which represents a typical single-photon entanglement between two temporal modes and will produce interference between $|10\rangle$ passing through the long arm and $|01\rangle$ the short arm. This interference is the origin of the RF's coherence.

To derive the AMZI output, we use port labelling as shown in Fig. 1b, Main Text. The transformation relation between input and output light field annihilation operators of the AMZI can be given by

$$\begin{aligned} a'_t &= \frac{1}{2} \{ [d_{t+\tau} + c_{t+\tau}] + e^{-i\varphi} [d_t - c_t] \}, \\ a'_{t-\tau} &= \frac{1}{2} \{ [d_t + c_t] + e^{-i\varphi} [d_{t-\tau} - c_{t-\tau}] \}. \end{aligned} \quad (\text{S.11})$$

The joint output quantum state of ports c and d at time t is the interference result of the RF state at times $t - \tau$

and t , see equation (S.10). Note that we have proved in Supplementary Section I that the attenuation along the optical path does not affect the RF's first-order coherence. Therefore, for clarity of expression, we treat the first beam splitter of the AMZI as a 3 dB attenuation without changing the form of the quantum state². For simple calculation and intuitive understanding, we use pure state analysis without considering channel loss and the first beam splitter of the AMZI. This treatment is equivalent to interfering the RF field with a delayed copy of itself, thus simplifying the derivation of the AMZI's output state. The simplified operator transformation relation is as follows (normalized)

$$\begin{aligned} a'_t &= \frac{1}{\sqrt{2}} e^{-i\varphi} [d_t - c_t], \\ a'_{t-\tau} &= \frac{1}{\sqrt{2}} [d_t + c_t]. \end{aligned} \quad (\text{S.12})$$

With the input state described in equation (S.10), the normalized output joint quantum state of ports c and d at time t then becomes

$$\begin{aligned} |\Psi_{\text{out}}\rangle_t &= |0_c 0_d\rangle_t \left(p_0 |gg\rangle + \frac{\sqrt{p_0 p_1}}{\sqrt{2}} |ge\rangle + \frac{\sqrt{p_0 p_1}}{\sqrt{2}} |eg\rangle + \frac{p_1}{2} |ee\rangle \right) \\ &+ |1_c 0_d\rangle_t \frac{\sqrt{p_0 p_1}}{\sqrt{2}} \frac{1 - e^{i\varphi}}{\sqrt{2}} |gg\rangle + |1_c 0_d\rangle_t \frac{p_1}{2\sqrt{2}} (|ge\rangle - e^{i\varphi} |eg\rangle) - |2_c 0_d\rangle_t e^{i\varphi} \frac{p_1}{2\sqrt{2}} |gg\rangle \\ &+ |0_c 1_d\rangle_t \frac{\sqrt{p_0 p_1}}{\sqrt{2}} \frac{1 + e^{i\varphi}}{\sqrt{2}} |gg\rangle + |0_c 1_d\rangle_t \frac{p_1}{2\sqrt{2}} (|ge\rangle + e^{i\varphi} |eg\rangle) + |0_c 2_d\rangle_t e^{i\varphi} \frac{p_1}{2\sqrt{2}} |gg\rangle, \end{aligned} \quad (\text{S.13})$$

when all RF photons are indistinguishable. The first line contains no photons, while the second and third lines represent complimentary outputs at ports c and d . Let's look just at port c . It contains a phase-dependent term $|1_c\rangle_t |gg\rangle$, corresponding to the TLE's transition from $(|ge\rangle + |eg\rangle)/\sqrt{2} \rightarrow |gg\rangle$. Varying the AMZI's phase φ , this term produces interference fringes with an amplitude of $\frac{p_0 p_1}{2}$. The remaining terms are non-interfering because $|1_c\rangle_t |ge\rangle$, $|1_c\rangle_t |eg\rangle$ and $|2_c\rangle_t |gg\rangle$ are projected onto different matter states. The corresponding transitions are from the same $|ee\rangle$ state, to different final states $|ge\rangle$, $|eg\rangle$ and $|gg\rangle$ respectively. The first two transitions correspond to the TLE emitting one photon into just one of the two temporal modes, while the last one means emitting one photon to each temporal mode and Hong-Ou-Mandel (HOM) interference produces the two-photon term $|2_c\rangle$. Altogether, these non-interfering terms contribute $\frac{p_1^2}{8} \times 2 + \frac{p_1^2}{4} = \frac{p_1^2}{2}$. Therefore, we obtain an interference fringe visibility as $\frac{p_0 p_1}{2} / (\frac{p_0 p_1}{2} + \frac{p_1^2}{2}) = p_0$, which is

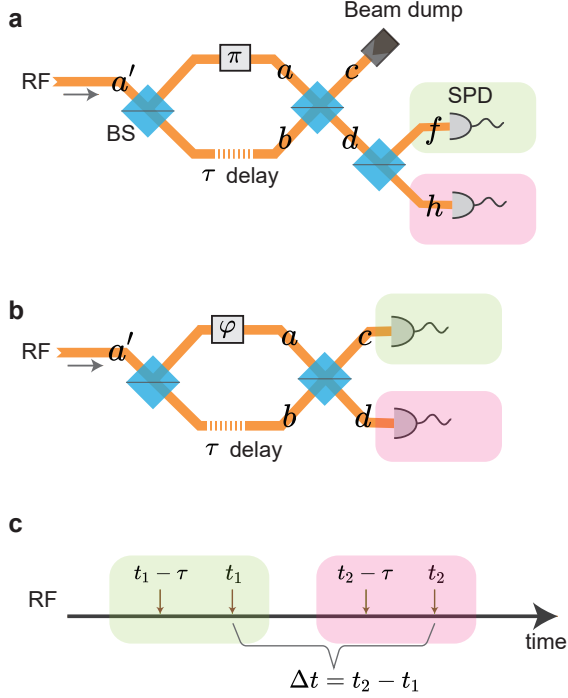
identical to the earlier result of equation (S.8). To sum up, the RF gains and loses its coherence both through spontaneous emission.

The discussion above is based on the assumption that single photons emitted by the TLE are perfectly indistinguishable. However, photons scattered out by the TLE underwent spontaneous emission processes, and therefore their indistinguishability would be degraded by the TLE's extrinsic scattering processes that are inherent in solid-state quantum systems. Taking into account of photon distinguishability, the first order coherence is revised accordingly to²

$$|g_{RF}^{(1)}(\tau)| = \sqrt{M} p_0, \quad (\text{S.14})$$

where M represents the indistinguishability of single photons between different temporal modes,

$$M = |\langle 1_t | 1_{(t-\tau) \rightarrow t} \rangle|^2, \quad (\text{S.15})$$



Supplementary Fig. 2. Phase-dependent second-order correlations. **a** $g^{(2)}(\Delta t)$ measurement setup for RF after π -phase AMZI filtering. **b**, HOM interferometer with a variable phase delay φ . **c**, Due to the AMZI delay τ , each coincidence count is related to up to four emission times at the RF source.

where $(t - \tau) \rightarrow t$ means delaying mode $t - \tau$ by τ for temporally overlapping $|1_t\rangle$ and $|1_{t-\tau}\rangle$.

IV. PHOTON SUPER-BUNCHING IN THE AMZI-FILTERED RF

According to equation (S.13), all the interfering single-photon fraction (laser-like) will exit from the port c if we set the AMZI's phase to $\varphi = \pi$. With the laser-like spectrum rejected, the port d will then contain two non-interfering single photon terms $|1_d\rangle|ge\rangle$ and $|1_d\rangle|eg\rangle$ as well as a two-photon term $|2_d\rangle|gg\rangle$. Measured with an auto-correlation setup as shown in Supplementary Fig. 2a, the port d output will exhibit super-bunching that arises from the two-photon term. Note this super-bunching is simply a result of two-photon interference and does not necessitate simultaneous scattering of two photons³ for an explanation.

In the HBT setup (Supplementary Fig. 2a), a coincidence event with f detector clicked at t_1 and h at t_2 involves the input of up to four non-degenerate temporal modes, t_1 , $t_1 - \tau$, t_2 and $t_2 - \tau$, see Supplementary Fig. 2c. Below, we will analyse the second-order correlation according to the level of their time degeneracy.

A. Non-degenerate

For interval $\Delta t = t_2 - t_1$ that meets both $|\Delta t \pm \tau| \gg T_1$ and $|\Delta t| \gg T_1$, there is no degeneracy in the four involved temporal modes. In Schrodinger picture, the second-order correlation function at $\Delta t \neq 0, \pm\tau$ is given by

$$\begin{aligned}
 g_{\varphi=\pi}^{(2)}(\Delta t) &= \frac{\langle \Psi_{\text{out}}|_{t_2} \langle \Psi_{\text{out}}|_{t_1} d_{t_2}^\dagger d_{t_1}^\dagger d_{t_1} d_{t_2} |\Psi_{\text{out}}\rangle_{t_1} |\Psi_{\text{out}}\rangle_{t_2}}{\langle \Psi_{\text{out}}|_{t_1} d_{t_1}^\dagger d_{t_1} |\Psi_{\text{out}}\rangle_{t_1}^2} \\
 &= \frac{\langle \Psi_{\text{out}}|_{t_2} d_{t_2}^\dagger d_{t_2} |\Psi_{\text{out}}\rangle_{t_2} \langle \Psi_{\text{out}}|_{t_1} d_{t_1}^\dagger d_{t_1} |\Psi_{\text{out}}\rangle_{t_1}}{\langle \Psi_{\text{out}}|_{t_1} d_{t_1}^\dagger d_{t_1} |\Psi_{\text{out}}\rangle_{t_1}^2} \\
 &= 1,
 \end{aligned} \tag{S.16}$$

where state $|\Psi_{\text{out}}\rangle_t$ is given by in equation (S.13) and $|\Psi_{\text{out}}\rangle_{t_1} |\Psi_{\text{out}}\rangle_{t_2}$ is the tensor product state between t_1 and t_2 .

B. Doubly degenerate: $t_1 = t_2$

At $\Delta t = 0$, the four temporal modes become doubly degenerate: $t_1 = t_2 = t$ and $t_1 - \tau = t_2 - \tau = t - \tau$. we work out the second-order correlation function for the 0-delay:

$$g_{\varphi=\pi}^{(2)}(0) = \frac{\langle \Psi_{\text{out}}| [d_t^\dagger]^2 d_t^2 |\Psi_{\text{out}}\rangle}{\langle \Psi_{\text{out}}| d_t^\dagger d_t |\Psi_{\text{out}}\rangle^2} = \frac{1}{p_1^2}. \tag{S.17}$$

We obtain super-bunching at 0-delay and it is excitation power dependent. The lower the excitation power, the higher the $g_{\varphi=\pi}^{(2)}(0)$ value becomes. At the limit of $\bar{n} \rightarrow 0$, $g_{\varphi=\pi}^{(2)}(0)$ can be infinitely large in theory. We emphasise again that this super-bunching does not require a higher-order scattering mechanism, contrary to previously suggested³.

C. Singly-degenerate: $t_2 - t_1 = \pm\tau$

For time intervals $t_2 - t_1 = \Delta t = \pm\tau$, three temporal modes at the AMZI input contribute to the coincidence at $\Delta t = \pm\tau$. For $\Delta t = \tau$, the corresponding modes are $t - \tau$, t and $t + \tau$. Input temporal mode t is split into two halves by the AMZI entrance beam splitter. The half passing through the short (long) arm interferes half of temporal mode $t - \tau$ ($t + \tau$) passing through the long (short) arm. At the AMZI output d , we just need to consider two temporal modes t and $t + \tau$ for calculating its $g^{(2)}(+\tau)$. We use the transformation relation (normalized) between output and input light field annihilation operators of the

AMZI with $\varphi = \pi$

$$\begin{aligned} d_t &= \frac{1}{\sqrt{2}} [a'_{t-\tau} - a'_t], \\ d_{t+\tau} &= \frac{1}{\sqrt{2}} [a'_t - a'_{t+\tau}], \end{aligned} \quad (\text{S.18})$$

where we ignore the loss by the first beam splitter. Using the Heisenberg picture, the second order correlation function can be derived using

$$g_{\varphi=\pi}^{(2)}(\tau) = \frac{\langle \psi_{\text{in}} | d_{t+\tau}^\dagger d_t^\dagger d_t d_{t+\tau} | \psi_{\text{in}} \rangle}{\langle \psi_{\text{in}} | d_t^\dagger d_t | \psi_{\text{in}} \rangle^2}. \quad (\text{S.19})$$

where operators evolve according to equation (S.18) and we have $|\psi_{\text{in}}\rangle = |\psi\rangle_{t-\tau} |\psi\rangle_t |\psi\rangle_{t+\tau}$. With time-evolving phases dropped for clarity, we have

$$d_t |\psi_{\text{in}}\rangle = \frac{1}{\sqrt{2}} [a'_{t-\tau} - a'_t] |\psi\rangle_{t-\tau} |\psi\rangle_t |\psi\rangle_{t+\tau} = \frac{p_1}{2\sqrt{2}} [|00\rangle (|ge\rangle + |eg\rangle) + (|01\rangle + |10\rangle) |gg\rangle] |\psi\rangle_{t+\tau}. \quad (\text{S.20})$$

and

$$\begin{aligned} d_t d_{t+\tau} |\psi_{\text{in}}\rangle &= \frac{1}{2} [a'_{t-\tau} - a'_t] [a'_t - a'_{t+\tau}] |\psi\rangle_{t-\tau} |\psi\rangle_t |\psi\rangle_{t+\tau} \\ &= \frac{p_1}{4} \left\{ \sqrt{p_0} |000\rangle |ggg\rangle + \frac{\sqrt{p_1}}{\sqrt{2}} [|000\rangle (|gge\rangle - |geg\rangle + |gge\rangle) + (|001\rangle - |010\rangle + |100\rangle) |ggg\rangle] \right\}. \end{aligned} \quad (\text{S.21})$$

We then obtain the second order correlation function at $\Delta t = \tau$:

$$g_{\varphi=\pi}^{(2)}(\tau) = \frac{p_1^2(1+2p_1)/16}{(p_1^2/2)^2} = \frac{1+2p_1}{4p_1^2}. \quad (\text{S.22})$$

Similarly, we derive the same conclusion for $\Delta t = -\tau$, i.e., $g_{\varphi=\pi}^{(2)}(\tau) = g_{\varphi=\pi}^{(2)}(-\tau)$. When $p_1 \ll 1$, we can have $1+2p_1 \approx 1$ and the second order interference coherence can be written as

$$g_{\varphi=\pi}^{(2)}(\pm\tau) \approx \frac{1}{4p_1^2} = \frac{1}{4} g_{\varphi=\pi}^{(2)}(0). \quad (\text{S.23})$$

V. PHASE-DEPENDENT HONG-OU-MANDEL INTERFERENCE

Hong-Ou-Mandel interferometry is an indispensable tool for evaluating indistinguishability among photons emitted by a pulsed single photon source⁴. As shown in Supplementary Fig. 2b, a typical HOM interferometer consists of an AMZI with a path difference of several nanoseconds and two single photon detectors. The AMZI's differential delay (τ) can bring two single photons separated by τ to temporally overlap for interference. If perfectly indistinguishable, two photons will coalesce and therefore the possibility for registering a photon simultaneously at each detector port is 0.

Continuous-wave HOM interference differs from the aforementioned results for pulsed single photons. The reason lies in the fact that when the detector's time resolution is arbitrarily high, unity indistinguishability would be obtained, i.e., $M = 1$, even if the two pho-

tons' spectral and temporal envelopes are not identical. More interestingly, in our experiments, due to the RF's long first-order coherence, coincidences of $\Delta t = \pm\tau$ are significantly different from those sources having short coherence times^{5,6}. As shown in Fig. 4 of the Main Text, we observe strong dependencies of the coincidence on the AMZI phase and excitation strength. Below, we give theoretical derivations of the coincidence $\mathcal{C}(\Delta t)$ for phase- and excitation power dependent HOM interference.

A. General description

As shown in Supplementary Fig. 2b, a quantum light input, now described by a density matrix ρ_t for convenience, enters the AMZI through port a' and is split equally into two paths a and b . With path a accumulating a phase of φ and path b a delay of τ , the split signals recombine at the exit 50/50 beam splitter to interfere. Photons exiting from ports c and d are detected by two single photon detectors. The transformation relation between output and input light field annihilation operators of the AMZI can be given by

$$\begin{aligned} c_t &= \frac{1}{2} [a'_{t-\tau} - e^{i\varphi} a'_t], \\ d_t &= \frac{1}{2} [a'_{t-\tau} + e^{i\varphi} a'_t], \end{aligned} \quad (\text{S.24})$$

where we have included the loss by the first beam splitter.

If we drop the phase $e^{i2\pi\nu t}$ in equation (S.7) that does not affect the result of the calculation, the density matrix

for describing the RF state can be written as

$$\frac{2p_0 + p_1}{2} |0\rangle \langle 0| + \frac{p_1}{2} |1\rangle \langle 1| + \sqrt{\frac{p_0 p_1}{2}} (|1\rangle \langle 0| + |0\rangle \langle 1|), \quad (\text{S.25})$$

after performing partial trace over system TLE. The resulting density matrix is equivalent to a pure state $|\phi\rangle = \sqrt{p_0}|0\rangle + \sqrt{p_1}|1\rangle$ after 3 dB channel loss and performing partial trace over the lost part. As we have proven in Section I that the channel loss does not affect the first and second order interference coherence, we can conveniently use the pure state $|\phi\rangle = \sqrt{p_0}|0\rangle + \sqrt{p_1}|1\rangle$ to calculate the coincidence probabilities in the HOM interference without loss of generality.

In the following derivation, we will use the pure state

$$|\phi_t\rangle = \sqrt{p_0}|0_t\rangle + \sqrt{p_1}|1_t\rangle + \sqrt{p_2}|2_t\rangle \quad (\text{S.26})$$

with $p_0 + p_1 + p_2 = 1$ and $p_2 \ll p_1^2/2$, instead of a mixture state density matrix as the incident light source for calculation. The introduction of the two-photon term $|2_t\rangle$ is to reflect the experimental setup imperfection that mixes a small amount of laser photons into the RF. The two-photon term is significant only for the calculation of the HOM dip.

B. Coincidence probability

A coincidence event with c detector clicked at t_1 and d at t_2 involves the input of up to four non-degenerate times, $t_1, t_1 - \tau, t_2$ and $t_2 - \tau$, see Supplementary Fig. 2c. Below, we will analyse their coincidence probabilities according to the level of their time degeneracy.

1. Non-degenerate

For intervals $\Delta t = t_2 - t_1$ that meets both $|\Delta t \pm \tau| \gg T_1$ and $|\Delta t| \gg T_1$, there is no degeneracy in the four involved times and each coincidence therefore is a result of two independent first-order interference events. For the incident quantum state, since the contribution of multi-photon components is small and has little impact on the final count, we consider only the lowest-order photon state $|1\rangle$ to capture the main characteristics of the baseline coincidence probability. The count probabilities

of detectors in ports c and d can be written as

$$\begin{aligned} \mathcal{P}_c &= \langle \phi_{t_1} | \langle \phi_{t_1 - \tau} | c_{t_1}^\dagger c_{t_1} | \phi_{t_1 - \tau} \rangle | \phi_{t_1} \rangle \\ &= |c_{t_1} | \phi_{t_1 - \tau} \rangle | \phi_{t_1} \rangle|^2 \\ &= \left| \frac{1}{2} [\sqrt{p_0 p_1} (1 - e^{i\varphi}) |00\rangle + p_1 (|01\rangle - e^{i\varphi} |10\rangle)] \right|^2 \\ &= \frac{p_1}{2} (1 - p_0 \cos \varphi), \end{aligned} \quad (\text{S.27})$$

and

$$\begin{aligned} \mathcal{P}_d &= \langle \phi_{t_2} | \langle \phi_{t_2 - \tau} | d_{t_2}^\dagger d_{t_2} | \phi_{t_2 - \tau} \rangle | \phi_{t_2} \rangle \\ &= \frac{p_1}{2} (1 + p_0 \cos \varphi), \end{aligned} \quad (\text{S.28})$$

where a'_{t_1} and $a'_{t_1 - \tau}$ act in quantum states $|\phi_{t_1}\rangle$ and $|\phi_{t_1 - \tau}\rangle$, respectively and state $|\phi_t\rangle = \sqrt{p_0}|0\rangle + \sqrt{p_1}|1\rangle$ after ignoring the two-photon component. Taking into account of imperfect photon indistinguishability defined in equation (S.15), we have

$$\begin{aligned} \mathcal{P}_c &= \frac{p_1}{2} (1 - \sqrt{M} p_0 \cos \varphi), \\ \mathcal{P}_d &= \frac{p_1}{2} (1 + \sqrt{M} p_0 \cos \varphi). \end{aligned} \quad (\text{S.29})$$

Consequently, the coincidence probability is simply the product of the count probabilities of individual detectors,

$$\mathcal{C}_0 = \mathcal{P}_c \mathcal{P}_d = \frac{p_1^2}{4} (1 - M p_0^2 \cos^2 \varphi). \quad (\text{S.30})$$

\mathcal{C}_0 the coincidence baseline depends on the AMZI's phase. At $\varphi = \pi/2$, it reaches its maximum.

Next we give a different deviation method to elaborate the correctness of equation (S.30). It will show the special properties of a continuous-wave RF, i.e., approximating the RF's quantum state as a coherent superposition of $|0\rangle$ and $|1\rangle$ is an acceptable treatment as long as the examined time interval is much larger than T_1 . Rigorously, its coincidence probability can be derived using^{2,7},

$$\begin{aligned} \mathcal{C}(\Delta t) &= \langle \psi_{\text{in}} | c_{t_1}^\dagger c_{t_1} d_{t_2}^\dagger d_{t_2} | \psi_{\text{in}} \rangle \\ &= \langle \psi_{\text{in}} | d_{t_2}^\dagger c_{t_1}^\dagger c_{t_1} d_{t_2} | \psi_{\text{in}} \rangle, \end{aligned} \quad (\text{S.31})$$

where $|\psi_{\text{in}}\rangle$ is the input quantum state and

$$c_{t_1} d_{t_2} = \frac{1}{4} [a'_{t_1 - \tau} - e^{i\varphi} a'_{t_1}] [a'_{t_2 - \tau} + e^{i\varphi} a'_{t_2}]. \quad (\text{S.32})$$

Let $t_1 = t$, then $t_2 = t + \Delta t$, which leads to

$$c_{t_1} d_{t_2} = c_t d_{t + \Delta t} = \frac{1}{4} [a'_{t - \tau} a'_{t + \Delta t - \tau} + a'_{t - \tau} a'_{t + \Delta t} e^{i\varphi} - a'_{t + \Delta t - \tau} e^{i\varphi} - a'_{t + \Delta t} e^{i2\varphi}]. \quad (\text{S.33})$$

Since there are four temporal modes involved in the above operator expression and the time interval between each

other is much larger than T_1 , the input quantum state can be expressed as a tensor product of the four temporal modes, i.e., $|\psi_{\text{in}}\rangle = |\phi_{t-\tau}\rangle |\phi_t\rangle |\phi_{t+\Delta t-\tau}\rangle |\phi_{t+\Delta t}\rangle$. Therefore,

$$\begin{aligned} & c_t d_{t+\Delta t} |\psi_{\text{in}}\rangle \\ &= \left[p_0 p_1 (-e^{i2\varphi} + e^{i\varphi} - e^{i\varphi} + 1) |0000\rangle + \sqrt{p_0 p_1^3} (1 + e^{i\varphi}) |0100\rangle \right. \\ & \quad + \sqrt{p_0 p_1^3} (-e^{i\varphi} - e^{i2\varphi}) |1000\rangle + \sqrt{p_0 p_1^3} (1 - e^{i\varphi}) |0001\rangle \\ & \quad \left. + \sqrt{p_0 p_1^3} (e^{i\varphi} - e^{i2\varphi}) |0010\rangle + p_1^2 |0101\rangle + p_1^2 e^{i\varphi} |0110\rangle - p_1^2 e^{i\varphi} |1001\rangle + p_1^2 e^{i2\varphi} |1010\rangle \right] / 4, \end{aligned} \quad (\text{S.34})$$

thereby

$$\mathcal{C}(\Delta t) = \langle \psi_{\text{in}} | d_{t_2}^\dagger c_{t_1}^\dagger c_{t_1} d_{t_2} | \psi_{\text{in}} \rangle = \frac{1}{4} p_0^2 p_1^2 \sin^2 \varphi + \frac{1}{2} p_0 p_1^3 + \frac{1}{4} p_1^4. \quad (\text{S.35})$$

Considering the influence of photon indistinguishability, $\mathcal{C}(\Delta t)$ should be corrected as

$$\begin{aligned} \mathcal{C}(\Delta t) &= \frac{1}{4} p_0^2 p_1^2 (1 - M \cos^2 \varphi) + \frac{1}{2} p_0 p_1^3 + \frac{1}{4} p_1^4 \\ &= \frac{1}{4} p_1^2 [(p_0 + p_1)^2 - M p_0^2 \cos^2 \varphi] \\ &= \frac{1}{4} p_1^2 [1 - M p_0^2 \cos^2 \varphi] = \mathcal{C}_0. \end{aligned} \quad (\text{S.36})$$

We obtain the same result as equation (S.30).

2. Singly-degenerate: $t_2 - t_1 = \pm \tau$

For intervals $\Delta t = \pm \tau$, two out of the four time slots become degenerate. Let's first consider $\Delta t = +\tau$. In this case, we write the operator corresponding based on equation (S.33),

$$c_t d_{t+\tau} = \frac{1}{4} [a'_{t-\tau} a'_t + e^{i\varphi} a'_{t-\tau} a'_{t+\tau} - e^{i\varphi} a'_t a'_t - e^{i2\varphi} a'_t a'_{t+\tau}]. \quad (\text{S.37})$$

Since the contribution of multi-photon components has negligible contribution to the coincidence at this delay, we use quantum state $|\phi_t\rangle = \sqrt{p_0} |0\rangle + \sqrt{p_1} |1\rangle$ to capture the main characteristics of the coincidence probability.

According to the expression of $c_t d_{t+\tau}$, the output state of the AMZI at time t is the interference result between the input state at time $t - \tau$ taking the long path and the input state at time t taking the short path. Accordingly, the output state of the AMZI at time $t + \tau$ is the interference result between the input state at time t taking the long path and the input state at time $t + \tau$ taking the short path. The input state for deriving $\mathcal{C}(+\tau)$, i.e., the coincidence probability at $+\tau$ interval between detectors c and d , should therefore be the tensor product of quantum states of three times $t - \tau$, t and $t + \tau$, i.e., $|\psi_{\text{in}}\rangle = |\phi_{t-\tau}\rangle |\phi_t\rangle |\phi_{t+\tau}\rangle$

$$c_t d_{t+\tau} |\phi_{t-\tau}\rangle |\phi_t\rangle |\phi_{t+\tau}\rangle = \frac{1}{4} \left[p_1 \sqrt{p_0} (1 + e^{i\varphi} - e^{i2\varphi}) |000\rangle + \sqrt{p_1^3} (|001\rangle + e^{i\varphi} |010\rangle - e^{i2\varphi} |100\rangle) \right], \quad (\text{S.38})$$

where $a'_{t+\tau}$, a'_t and $a'_{t-\tau}$ act on states $|\phi_{t-\tau}\rangle$, $|\phi_t\rangle$, and $|\phi_{t+\tau}\rangle$, respectively. We then obtain the coincidence probability

$$\mathcal{C}(\tau) = \frac{1}{16} p_0 p_1^2 (3 - 2 \cos 2\varphi) + \frac{3}{16} p_1^3. \quad (\text{S.39})$$

imperfect photon indistinguishability, $\mathcal{C}(\pm \tau)$ is corrected to

$$\mathcal{C}(\pm \tau) = \frac{1}{16} p_0 p_1^2 (3 - 2M \cos 2\varphi) + \frac{3}{16} p_1^3. \quad (\text{S.40})$$

For $\Delta t = -\tau$, one can follow the same derivation process and obtain $\mathcal{C}(-\tau) = \mathcal{C}(+\tau)$. Taking into account of

3. Doubly degenerate: $t_1 = t_2$

At $\Delta t = 0$, the four time slots (Supplementary Fig. 2c) become doubly degenerate: $t_1 = t_2 = t$ and $t_1 - \tau = t_2 - \tau = t - \tau$. Coincidence at this interval has two contributions: (1) multi-photon components in the input and (2) imperfect two-photon interference. As these two contributions are on the same magnitude, it is necessary to include the two-photon term in the input state in order to derive the correct coincidence probability. We use the pure state $|\phi_t\rangle = \sqrt{p_0}|0\rangle + \sqrt{p_1}|1\rangle + \sqrt{p_2}|2\rangle$ as the input.

Following equation (S.33), the operator for $\Delta t = 0$ and $t_1 = t_2 = t$ can be written as

$$c_t d_t = \frac{1}{4} \left[a'_{t-\tau} a'_{t-\tau} - e^{i2\varphi} a'_t a'_t + \underline{e^{i\varphi} a'_{t-\tau} a'_t} - \underline{e^{i\varphi} a'_t a'_{t-\tau}} \right], \quad (\text{S.41})$$

$$\begin{aligned} c_t d_t |\phi_{t-\tau}\rangle |\phi_t\rangle = & \frac{1}{4} \left\{ \left[\sqrt{2p_0 p_2} (1 - e^{i2\varphi}) + \underline{p_1 e^{i\varphi}} - \underline{p_1 e^{i\varphi}} \right] |00\rangle + \sqrt{2p_1 p_2} (1 + \underline{e^{i\varphi}} - \underline{e^{i\varphi}}) |01\rangle \right. \\ & + \sqrt{2p_1 p_2} (\underline{e^{i\varphi}} - \underline{e^{i\varphi}} - e^{i2\varphi}) |10\rangle + 2p_2 (\underline{e^{i\varphi}} - \underline{e^{i\varphi}}) |11\rangle \\ & \left. + \sqrt{2p_2} (|02\rangle - e^{i2\varphi} |20\rangle) \right\}, \end{aligned} \quad (\text{S.42})$$

where $a'_{t-\tau}$ and a'_t act in quantum states $|\phi_{t-\tau}\rangle$ and $|\phi_t\rangle$ respectively. If photons are all identical, all underlined terms cancel out, leading to

$$C(0) = \frac{1}{4} p_0 p_2 (1 - \cos 2\varphi) + \frac{1}{4} p_1 p_2 + \frac{1}{4} p_2^2 = \frac{p_2}{4} (1 - p_0 \cos 2\varphi). \quad (\text{S.43})$$

When considering finite photon indistinguishability defined in equation (S.15), all terms that depend on φ must be corrected accordingly and we then obtain

$$C(0) = \frac{p_2}{4} (1 - p_0 M \cos 2\varphi) + \frac{p_1^2 + 4p_1 p_2 + 4p_2^2}{8} (1 - M'), \quad (\text{S.44})$$

where M' has similar definition as M but further takes into account for the detector time resolution. Effectively, we let $|\underline{e^{i\varphi}} - \underline{e^{i\varphi}}|^2 = 2(1 - M')$ in obtaining equation (S.44).

VI. EXPERIMENTAL SETUP

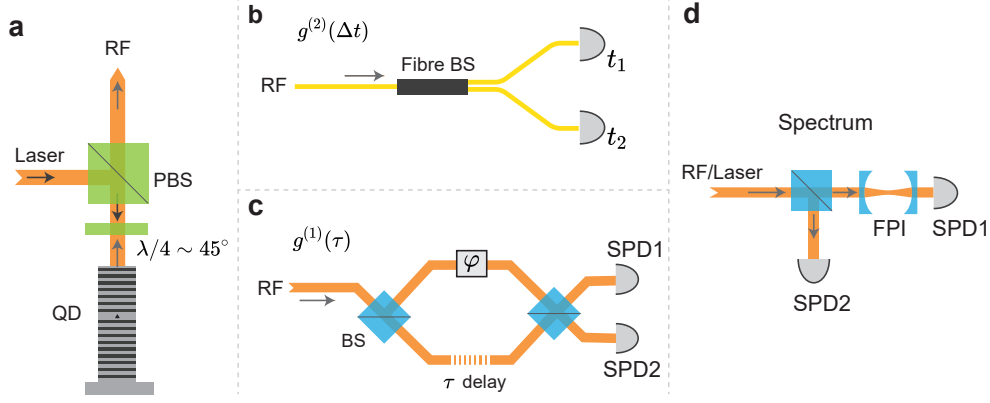
The main experimental apparatus is shown in Supplementary Fig. 3a. Here, a polarising beam splitter (PBS) and a $\sim 45^\circ$ quarter-wave plate are used together as an optical router to direct the RF from the quantum dot (QD) to the measurement apparatuses shown in panels **b**, **c** and **d**. A continuous-wave excitation laser (M SQUARED SolsTis PSX XF 5000, with a linewidth of ~ 100 kHz) is used as the excitation source. Unlike typical RF setups^{5,6}, the reflected laser and the RF in our experiment have the same polarisation, thanks to our

where the first two terms produce interference between an early two-photon state taking the long arm and a late two-photon state passing the short arm, while the underlined terms cause two-photon HOM interference between an early and a late single photon. If photons are not identical and the detector resolution is limited, the output by the underlined terms will not cancel completely. According the above equation, we only need to consider the states of two input temporal modes $t - \tau$ and t , i.e., $|\psi_{\text{in}}\rangle = |\phi_{t-\tau}\rangle |\phi_t\rangle$ leading to

microcavity design⁸ that minimises the laser reflection to have negligible impacts on the measurements.

Supplementary Fig. 3b shows a standard Hanbury-Brown Twiss (HBT) setup for measuring the auto-correlation function $g^{(2)}(\Delta t)$ that evaluates the single-photon purity of the input signal. It consists of a 50:50 fibre beam splitter and two single photon detectors. An ideal single-photon state corresponds to $g^{(2)}(0) = 0$.

Supplementary Fig. 3c illustrates a setup for characterising the first-order correlation function $g^{(1)}(\tau)$. In this setup, both beam splitters have a nominal 50:50 reflectance-to-transmittance ratio, and the AMZI's differential delay is 4.92 ns. The count rates at the detectors oscillate with a free-drifting phase φ . By measuring the maximum and minimum values of this oscillation, we can calculate the interference fringe visibility: $V \equiv |g^{(1)}(\tau)| = \frac{C_{\text{max}} - C_{\text{min}}}{C_{\text{max}} + C_{\text{min}}}$. Usually, one detector would suffice. However, to avoid the QD blinking affecting the measurement result, we use a two-channel summation method to normalise each detector's count rate to the combined count rate for the visibility calculation. In the super-bunching (Fig. 3, Main Text) and phase-dependent two-photon interference (Fig. 4, Main Text) experiments, the phase of the AMZI is stabilised to a set value for every measurement.



Supplementary Fig. 3. Experimental setup. **a**, Coherent single photon source generation device. **b**, Fibre beam splitter for $g^{(2)}(\Delta t)$ measurement. **c**, Mach-Zehnder interferometer for $g^{(1)}(\tau)$ measurement. **d**, Setup for the spectrum measurement of RF or excitation laser.

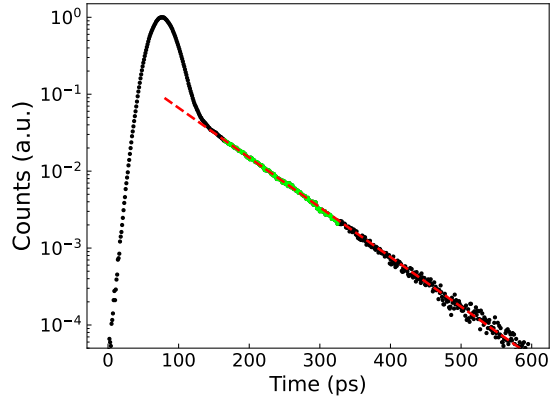
Supplementary Fig. 3d is the setup for measuring the RF frequency spectrum. The RF signal is split into two paths. One path enters the scanning Fabry-Pérot Interferometer (FPI) with a single photon detector (SPD1) recording the signal count rate as a function of the FPI transmission frequency, which is controlled by a piezo actuator. The other path enters a second single photon detector (SPD2) for normalising SPD1's detection results. The scanning FPI has a free spectral range of 20 GHz and a resolution of 20 MHz.

Two superconducting nanowire single photon detectors (SNSPDs) are used for single photon detection. These SNSPDs are characterised to have a single-photon detection efficiency of 78 % and a time jitter of 48 ps at the

wavelength of 910 nm. A time-tagger is used for correlation and time-resolved measurements.

Our sample consists of a λ -GaAs layer contain single layer of low-density In(Ga)As QDs sandwiched between two distributed Bragg reflectors formed by 18 (top) and 30.5 (bottom) GaAs/ $\text{Al}_{0.9}\text{Ga}_{0.1}\text{As}$ layer pairs. Using scanning reflectance spectroscopy, we determine the resonance of the HE_{11} cavity mode to have a central wavelength of 911.54 nm and a linewidth of 0.0975 nm ($\kappa = 35$ GHz), corresponding to a quality factor (Q) of approximately 9350. Using a picosecond Ti:S laser, the QD exciton lifetime is characterised to be 67.2 ps, see Supplementary Fig. 4, which corresponds to a radiative linewidth of $\Gamma_{\parallel}/2\pi = 2.37$ GHz.

1. Steck, D. A. Quantum and atom optics. <http://steck.us/teaching> (revision 0.14, 23 August 2023).
2. Lored, J. *et al.* Generation of non-classical light in a photon-number superposition. *Nat. Photon.* **13**, 803–808 (2019).
3. Masters, L. *et al.* On the simultaneous scattering of two photons by a single two-level atom. *Nat. Photon.* **17**, 972–976 (2023).
4. Santori, C., Fattal, D., Vučković, J. & Yamamoto, Y. Indistinguishable photons from a single-photon device. *Nature* **419**, 594 – 597 (2002).
5. Proux, R. *et al.* Measuring the photon coalescence time window in the continuous-wave regime for resonantly driven semiconductor quantum dots. *Phys. Rev. Lett.* **114**, 067401 (2015).
6. Patel, R. B. *et al.* Postselective two-photon interference from a continuous nonclassical stream of photons emitted by a quantum dot. *Phys. Rev. Lett.* **100**, 207405 (2008).
7. Legero, T., Wilk, T., Kuhn, A. & Rempe, G. Time-resolved two-photon quantum interference. *Appl. Phys. B* **77**, 797–802 (2003).
8. Wu, B. *et al.* Mollow triplets under few-photon excitation. *Optica* **10**, 1118 – 1123 (2023).



Supplementary Fig. 4. Exciton lifetime of the QD.

The black dots represent the time evolution of the measured intensity reflected by the device using pulsed excitation. The primary rapid decay is attributed to the instrument response caused by the residual laser pulse. The green dots are extracted to fit the exciton lifetime and the red dashed line is the fitted curve, which gives the exciton lifetime of 67.2 ps.